Available online at www.sciencedirect.com
ScienceDirect
Polymer 49 (2008) 2160–2169
polymer
www.elsevier.com/locate/polymer

Pendulum-like motion of straight electrified jets

Tao Han [a], Darrell H. Reneker [a,*], Alexander L. Yarin [b]

[a] Department of Polymer Science, The University of Akron, Akron, Ohio 44325-3909, United States
[b] Department of Mechanical and Industrial Engineering, University of Illinois at Chicago, Chicago, Illinois 60607-7022, United States

Received 4 October 2007; received in revised form 18 January 2008; accepted 19 January 2008
Available online 29 January 2008

Abstract

A novel phenomenon, a pendulum-like motion of the usually straight electrified jet was observed experimentally and theoretically modeled. Pendulum-like motion arises due to repulsive Coulomb force between the straight electrified jet and the charges accumulated on the collector. This electrical force repels the similarly charged landing jet segment in the collector plane. The motion is transferred to the whole jet via elastic stress sustained by the jet. The initially straight segment of the jet is arched. The pendulum-like motion has frequencies of the order of 10–10^2 Hz. The pendulum-like jets were collected onto grounded horizontal electrodes moving laterally at a constant velocity or being at rest. Different two-dimensional patterns were produced by varying the applied voltage, the separation between the tip and collector and the velocity vector of the collector.
© 2008 Elsevier Ltd. All rights reserved.

Keywords: Electrospinning; Pendulum motion; Nanofibers

1. Introduction

Straight electrified jets of low viscosity Newtonian liquids were investigated experimentally and theoretically since the end of the 19th century, mostly on the effect of the electric field on the capillary instability [1–7]. Later on, when electrically-driven jets of highly viscous Newtonian liquids or of viscoelastic polymer solutions came into focus, a number of experimental and theoretical papers aimed at prediction of the tapering shape of such straight jets [8–14]. In addition it was discovered that straight electrified jets can become unstable to the electrically-driven bending perturbations and make large, rapidly evolving loops which elongate rapidly the thin liquid jet in the industrially important process called electrospinning of polymer nanofibers [10,15–21]. Other electrically-driven instabilities leading to jet branching were theoretically predicted and observed in the experiments [10,22,23]. Buckling of electrified straight and bending jets was also studied [24].

A new phenomenon characteristic of electrified jets is described here. It is shown that for short enough jets, when bending instability is absent, the usually straight segment arched in a radial plane and rotated as a pendulum. Section 2 describes the experimental setup and materials used. Section 3 presents the experimental results. A theoretical model is proposed in Section 4. Theoretical results and comparison with the experimental data are contained in Section 5. Conclusions are drawn in Section 6.

2. Experimental

2.1. Materials

Nylon-6, 25 wt% solution in formic acid, (FA), 88%. All chemicals were purchased from Sigma–Aldrich Co.

2.1.1. Experimental setup

The experimental setup (Fig. 1) for electrospinning was similar to those used previously [10,15,21,24]. The collector was either motionless or moved horizontally at a constant speed of $V_c = 0–0.01$ m/s. Also, in some experiments a grounded liquid surface was used as collector.

* Corresponding author. Tel.: +1 330 972 6949; fax: +1 330 972 5461.
E-mail address: reneker@uakron.edu (D.H. Reneker).

0032-3861/$ - see front matter © 2008 Elsevier Ltd. All rights reserved.
doi:10.1016/j.polymer.2008.01.048

Nomenclature

a	The radius of the previously deposited fiber mat
b	Cross-sectional radius of the jet
C	Volumetric charge density in the jet
D	Diameter of the jet deposit
D_1, D_2	The dimensionless groups in Eqs. (2) and (3)
e	The electric charge on the recently landed segment of the jet
E	Young's modulus
$E(\mu)$ and $K(\mu)$	The complete elliptic integrals
f	The dimensionless group in Eq. (7)
$\mathbf{F}$	The Coulombic repulsive force acting on the landed segment of the jet
H	The tip to collector distance
H_1	The dimensionless tip to collector distance ($H_1 = H/a$)
I	Moment of inertia of the jet cross-section
I_{el}	The electrical current carried by the jet
$\mathbf{i}$, $\mathbf{j}$	The unit vectors of x and y axes
ℓ	The length of the landing section of the jet
L	The jet length
m	The jet mass
P	The dimensionless group in Eqs. (2) and (3)
q	The linear charge density
q_0	The linear charge density without charge relaxation
Q	The dimensionless parameter characterizing the ratio of the electrical and elastic forces
t	Time
T	The time scale
V	Jet velocity
$V_{jet\ end}$	The landing velocity of the jet end
V_x, V_y	The velocity components of the landed jet segment
x,y,z	The Cartesian coordinates (x and y are in the electrode plane, z-normal to it)
X,Y,Z	The coordinates of the jet elements in space
α	The angular coordinate of the jet plane
β	The whole envelope angle about the electrified jet
γ	Dummy variable
ε	The electrical permittivity
θ	Polar angle in the electrode plane
Θ	The viscoelastic relaxation time
μ	The dimensionless group in Eqs. (2) and (3)
μ_{el}	The elongational viscosity
ξ	The radial coordinate of a jet element in space
ξ_0	The radial polar coordinate of the landed jet segment
ρ	Polymer solution density
σ	The electrical conductivity
τ	Charge relaxation time
ω	Rotation frequency of the pendulum-like motion

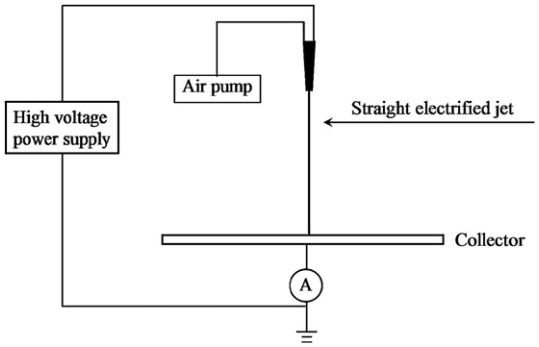

Fig. 1. Schematic representation of the experimental setup.

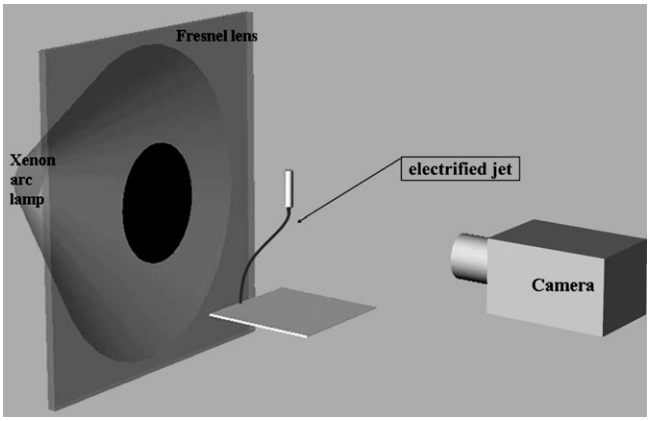

Fig. 2. Setup for the observation of the jet.

The experiments were conducted under ambient conditions at room temperature and a relative humidity of about 25%. Polymer solutions were held in a glass pipette which had an inner diameter of 800 μm. A copper wire was immersed in the solution and connected to a high voltage power supply which generated DC voltage up to 13 kV. No syringe pump was used. The flow was controlled by the outward electrical Maxwell stresses and the air pressure or partial vacuum applied to the surface of the liquid in the pipette. The distance between the pipette tip and the collector, along the straight vertical line, could be adjusted from 1 to 55 mm. An ammeter was connected between the collector and electrical ground to measure the current carried by the jet.

A high frame rate camera attached to an optical microscope was used to record the morphology of the jet (Fig. 2). The Fresnel lens produced a converging cone of illumination at the location of the electrified jet. The opaque disk on the Fresnel lens prevented direct rays of light from the arc lamp from entering the camera. Light scattered by the jet entered the camera and allowed observation of the jet path.

3. Experimental results

The nylon-6 fibers were collected on the collector which was motionless or moved laterally with a speed of 0.001 m/s or 0.01 m/s. The tip to collector distances were small, not more than 55 mm. Therefore, the jet stayed straight or was collected as almost straight and did not develop any large scale coils of increasing diameter that are a consequence of the

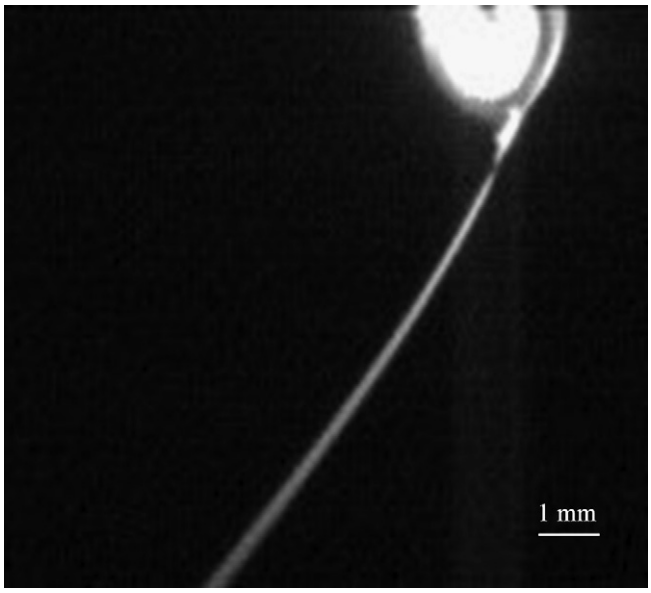

Fig. 3. A selected frame from a high frame rate video image of a pendulum-like electrified jet near the collecting surface. The voltage was 3 kV and the tip to collector distance was 26 mm.

bending instability in electrospinning [10]. The jet began swinging and rotating as a pendulum, following an almost periodic, circular and closed trajectory on the grounded electrode. A stopped motion view near the tip of the pendulum-like jet is shown in Fig. 3. The closed trajectories of the jet on the grounded electrode were almost circular. When the electrode was moved laterally, a family of such circles intersecting each other was deposited (Fig. 4). Sharpness of the edges of the deposited lines depended on the tip to collector distance and the applied voltage (cf. Figs. 4 and 5). When the tip to collector distance was increased from 8 to 30 mm at a fixed voltage of 4 kV (Figs. 5–8), the jet segments impacting the grounded electrode became thin enough for buckling to occur [24]. Then, the deposited circular lines on the grounded electrode acquired a small-scale zigzag-like structure, which varied as tip to collector distance became larger (Figs. 6–8).

Figs. 9–13 contain information on the electrified jets moving as a pendulum under different conditions. Fig. 9 depicts the electrical current transferred by the jets to the grounded electrode versus the tip to collector distance H for several values of the applied voltage in the range of 3–6 kV. A similar dependence for the whole angle at the vertex of the region inside the volume defined by the rotation of the pendulum jet is shown in Fig. 10. The angle was measured from the pictures taken by the high frame rate video camera.

The frequency of the pendulum-like motions of the electrified jets at different tip to collector distances and voltages are combined in Fig. 11. The frequency was measured from the sequence of the pictures recorded by the high frame rate video camera.

Diameters D of the collected patterns and arrival velocities of the jet $V_{\text{jet end}}$ versus the tip to collector distance H for different values of the applied voltage are presented in Figs. 12

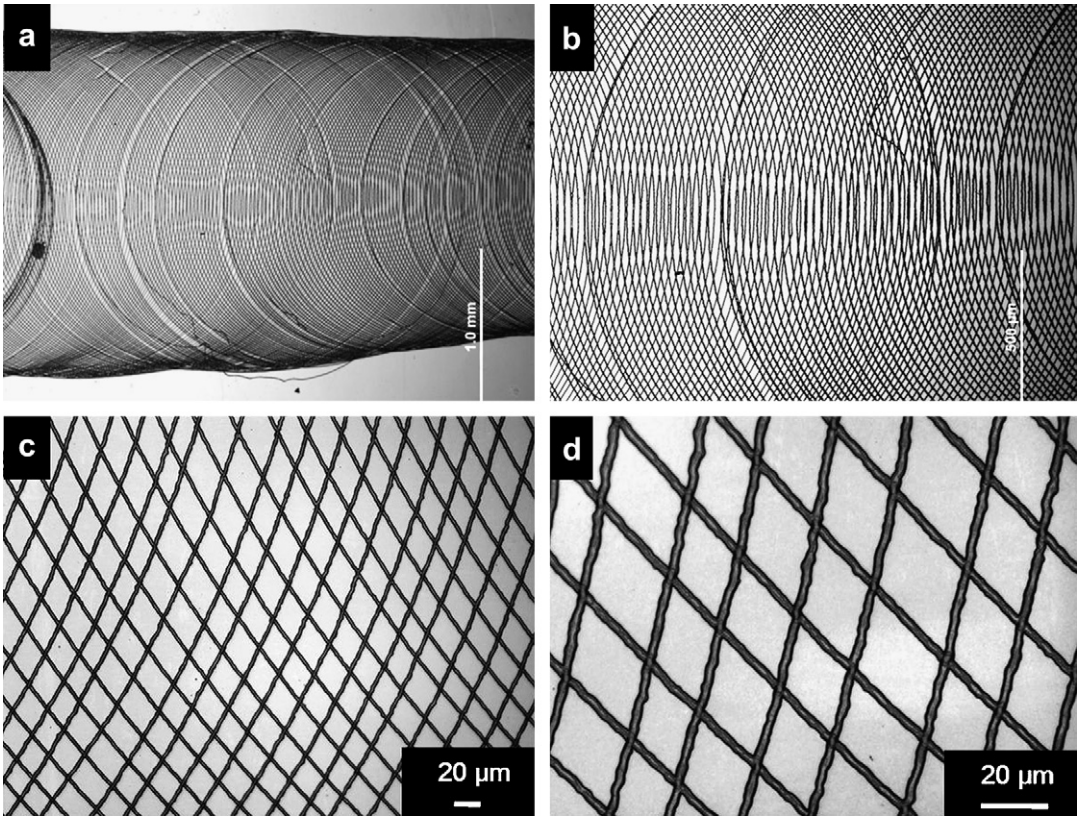

Fig. 4. Optical microscopic images of patterns deposited by an electrified jet moving as a pendulum. The voltage was 3 kV, the tip to collector distance was 5 mm; the grounded electrode was moved horizontally at 0.001 m/s.

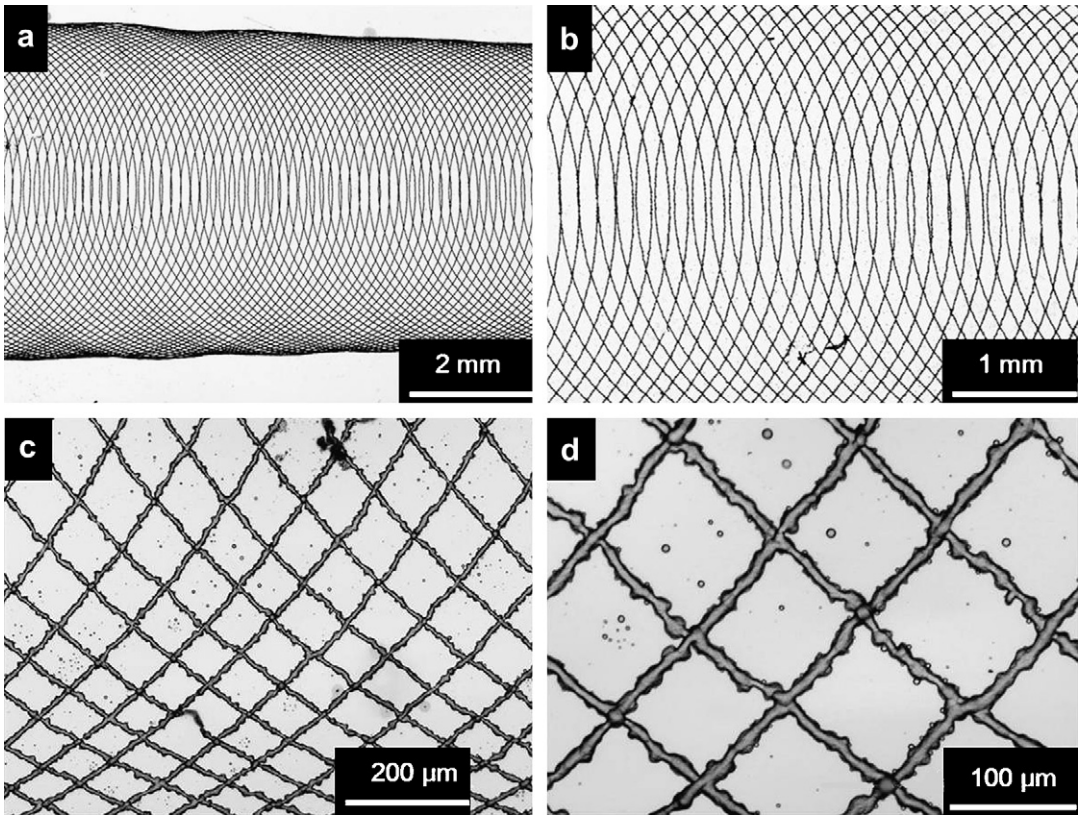

Fig. 5. Optical microscopic images of patterns produced from an electrified jet moving as a pendulum. The voltage was 4 kV, the tip to collector distance was 8 mm; the grounded electrode was moved horizontally at 0.01 m/s.

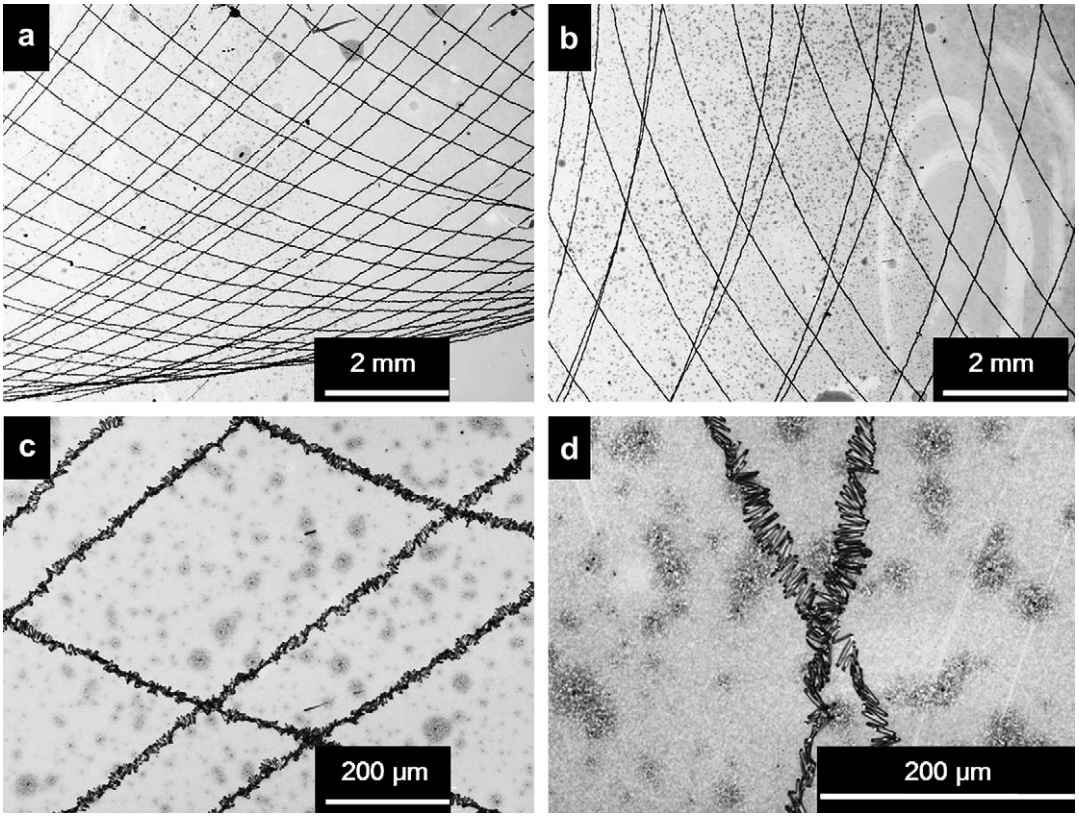

Fig. 6. Optical microscopic images of patterns produced from an electrified jet moving as a pendulum. The voltage was 4 kV, the tip to collector distance was 18 mm; the grounded electrode was moved horizontally at 0.01 m/s.

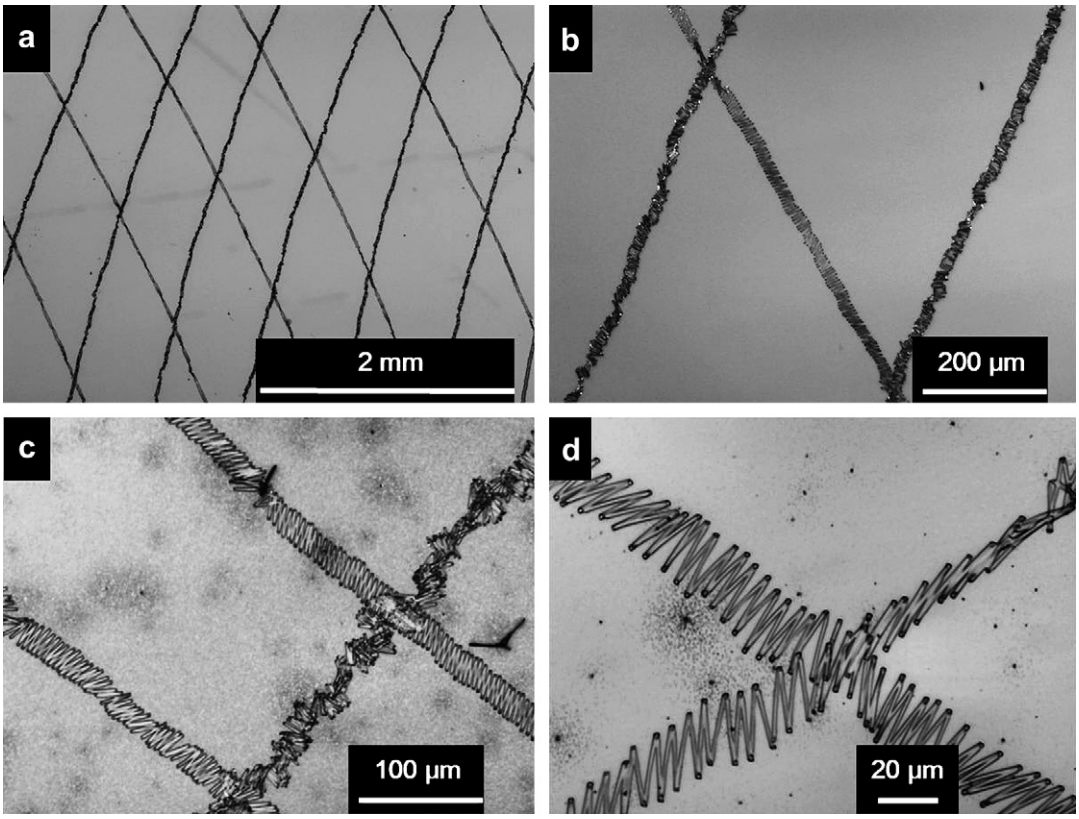

Fig. 7. Optical microscopic images of patterns produced from an electrified jet moving as a pendulum. The voltage was 4 kV, the tip to collector distance was 20 mm; the grounded electrode was moved horizontally at 0.01 m/s.

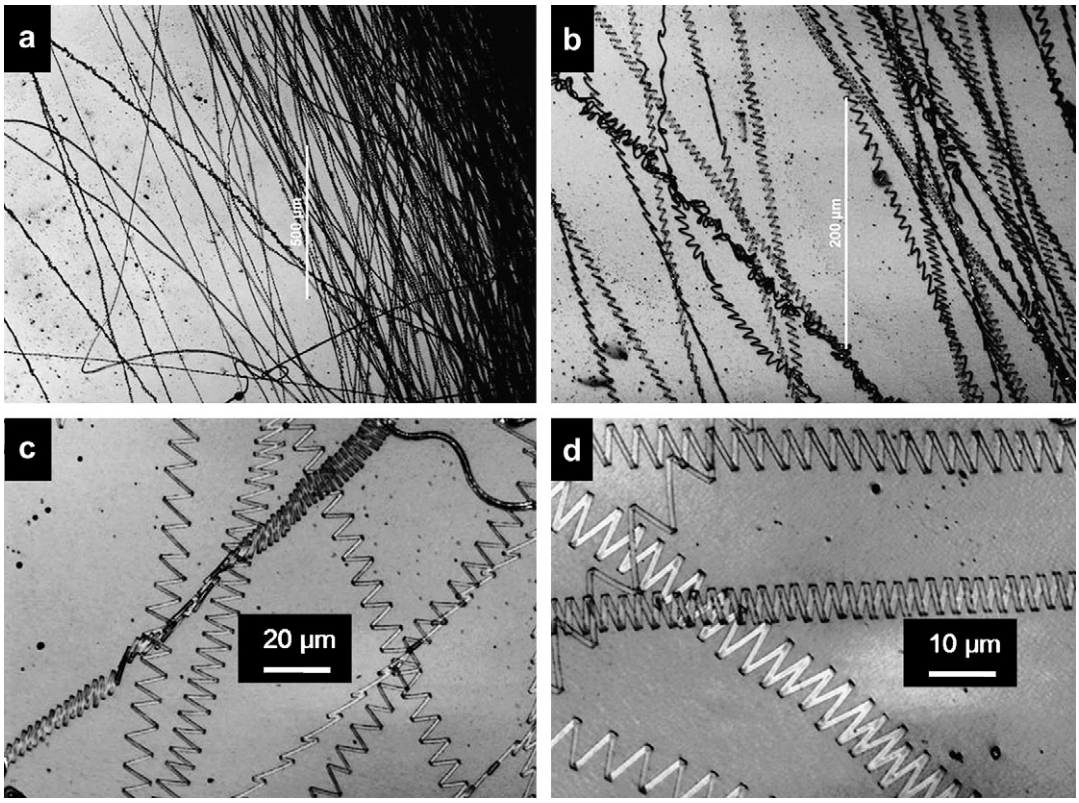

Fig. 8. Optical microscopic images of patterns produced from an electrified jet moving as a pendulum. The nylon-6 fibers were collected on a static water surface which served as a grounded electrode. The voltage was 4 kV, and the tip to collector distance was 30 mm.

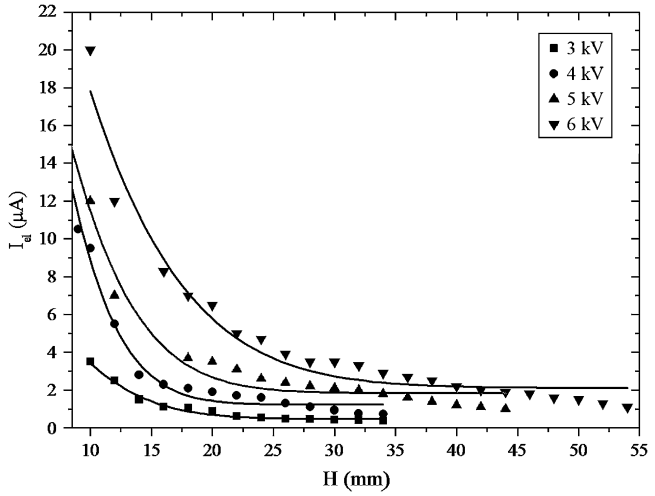

Fig. 9. The electrical current carried by the electrified jets as a function of the tip to collector distance for different applied electrical voltages. A horizontal, motionless, aluminum sheet was used as a grounded collector electrode.

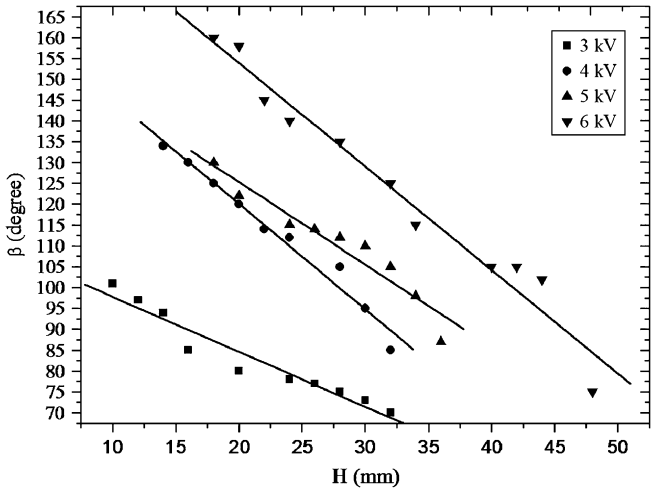

Fig. 10. The whole angle of the conical region that contained the configurations of the electrified pendulum-like jets as a function of the tip to collector distance for different applied electrical voltages. A horizontal motionless aluminum sheet was used as a grounded collector electrode.

and 13, respectively. $V_{\text{jet end}}$ was calculated from the measured pendulum frequency and diameter of the collected coils as $V_{\text{jet}} = \omega\pi D$.

4. Theoretical model

The electrical charge delivered by an electrified jet to the grounded electrode can relax, that is, move from the landing site of the jet to the metal collector on a time scale of the order of $\tau = \varepsilon/(4\pi\sigma)$, where ε and σ are the effective electrical permittivity and conductivity, respectively, of the collected fibers (Gaussian units are used). The previously collected charged fibers are assumed to form disc of radius a. The disappearance of the charge is not immediate and some charge can remain for long times on collected fibers that have low electrical conductivity. The linear charge density over the disc perimeter is q. In the following, the charge on the far away segments of the

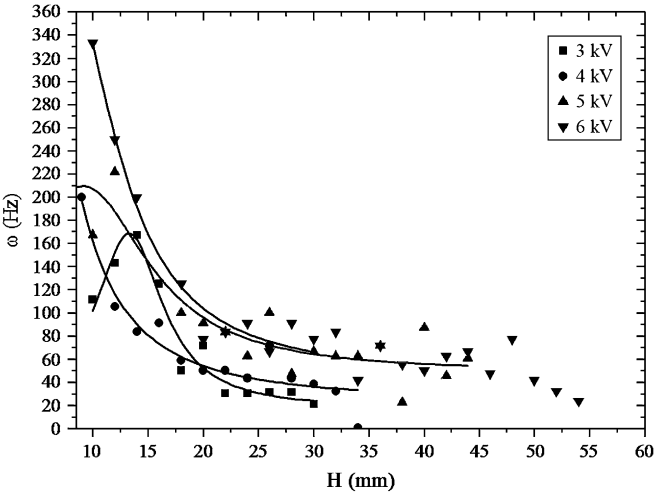

Fig. 11. Rotational frequency ω of the pendulum-like motion of the electrified jets as a function of the tip to collector distance for different applied electrical voltages. A horizontal, motionless, aluminum sheet was used as a grounded collector electrode.

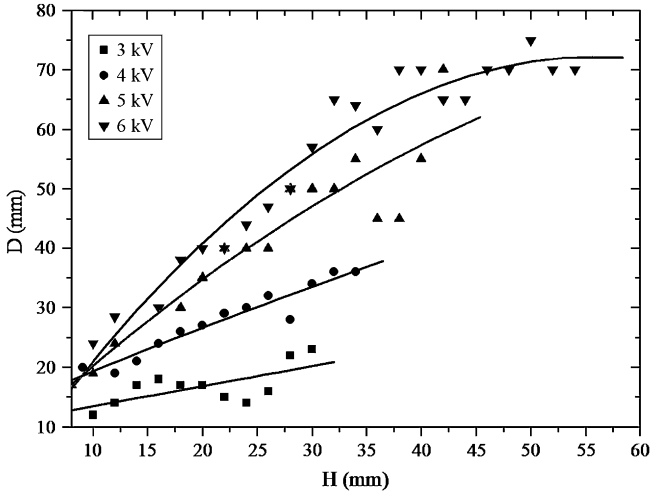

Fig. 12. Diameter of the collected circular deposits of the electrified jets as a function of tip to collector distance for different applied electrical voltages. A horizontal, motionless, aluminum sheet was used as a grounded collector electrode.

oncoming jet will be neglected compared to the charge at the most recently landed segment, which delivered the electric charge denoted as e. A schematic drawing of the pendulum-like motion of the electrified jet is shown in Fig. 14.

Using the Cartesian coordinates xyz centered at the disc center as well as the azimuthal angle θ corresponding to points on the disc edge, the Columbic repulsive force $\mathbf{F}$ acting at the jet segment in contact with the disc is given as

$$\mathbf{F} = qea \int_0^{2\pi} \frac{\mathbf{i}(x - a\cos\theta) + \mathbf{j}(y - a\sin\theta)}{\left[(x - a\cos\theta)^2 + (y - a\sin\theta)^2\right]^{3/2}} \mathrm{d}\theta \qquad (1)$$

where it is assumed that the disc is located at $z = 0$ with z being the coordinate axis normal to the disc plane; $\mathbf{i}$ and $\mathbf{j}$

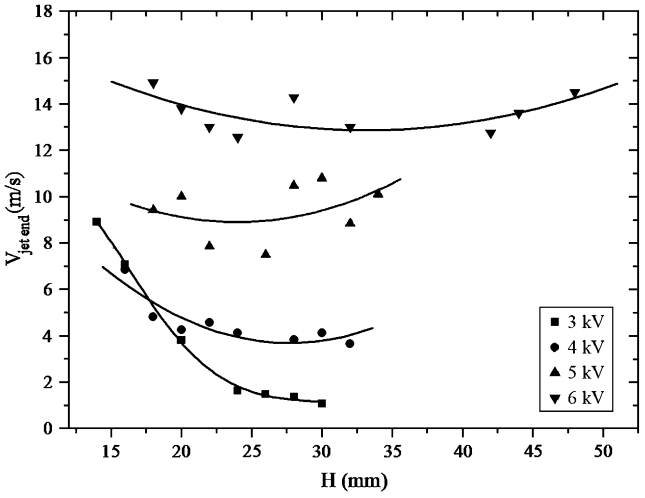

Fig. 13. The arrival velocity of the electrified jets as a function of the tip to collector distance for different values of the applied electrical voltages. A horizontal, motionless, aluminum sheet was used as a grounded collector electrode.

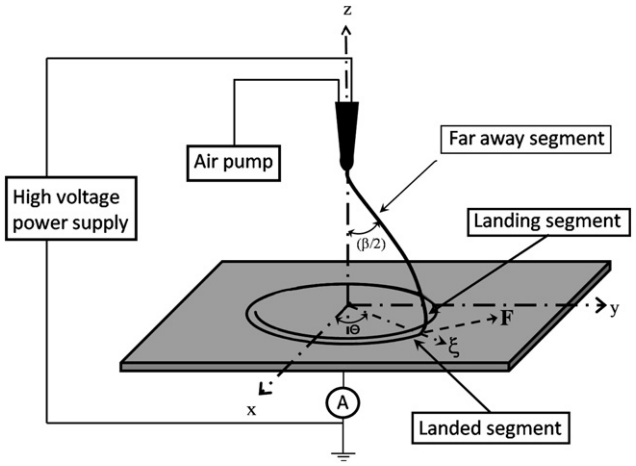

Fig. 14. Schematic representation of the pendulum-like motion of the electrified jet.

are the unit vectors of x and y axes in the disc plane, respectively.

The integral in Eq. (1) can be expressed through the complete elliptic integrals. Then the components of the repulsive electric force acting on a landed jet segment (with charge e) from the unrelaxed electric charge present at the disc edge (with linear density q) are given by the following dimensionless expressions

$$\begin{aligned} \mathrm{F}_x &= x\frac{4E(\mu)}{D_2^{3/2}(1-\mu)} - \frac{x}{(x^2+y^2)^{1/2}}P, \\ \mathrm{F}_y &= y\frac{4E(\mu)}{D_2^{3/2}(1-\mu)} - \frac{y}{(x^2+y^2)^{1/2}}P \end{aligned} \tag{2}$$

where the force components are rendered dimensionless by qe/a and the coordinates (x, y) by a,

$$\begin{aligned} &D_1 = x^2+y^2+1, \quad D_2 = \left[(x^2+y^2)^{1/2}+1\right]^2, \\ &\mu = \frac{4\left(x^2+y^2\right)^{1/2}}{D_2}, \\ &P = \frac{2D_1E(\mu)}{D_2^{3/2}(x^2+y^2)^{1/2}(1-\mu)} - \frac{2K(\mu)}{D_2^{1/2}(x^2+y^2)^{1/2}} \end{aligned} \tag{3}$$

In Eqs. (2) and (3) $E(\mu)$ and $K(\mu)$ denote the complete elliptic integrals [25].

The electrical repulsive force pushes the landing segment in the disc plane. The resulting motion is transferred to the whole jet via the elastic stresses sustained by polymer solutions. As a result, the whole jet moves under the action of the electric force acting on its landing segment. Note that the landing segment must be large compared to the characteristic scale of the buckling phenomena observed, since the theory does not include any buckling phenomena. The equations of motion of the landing segment under the action of the electrical repulsive force from the disc edge have the following dimensionless form

$$\frac{\mathrm{d}x}{\mathrm{d}t} = V_x, \quad \frac{\mathrm{d}y}{\mathrm{d}t} = V_y, \quad \frac{\mathrm{d}V_x}{\mathrm{d}t} = \mathrm{F}_x, \quad \frac{\mathrm{d}V_y}{\mathrm{d}t} = \mathrm{F}_y \tag{4}$$

with the components of force determined in Eqs. (2) and (3). In Eq. (4) time is rendered dimensionless by $T = [ma^2/(qe)]^{1/2}$, where m is the mass of the whole jet; the velocity components V_x and V_y are rendered dimensionless by a/T.

Eq. (4) is solved numerically. Its solution determines the coordinates of the landed jet segment on the disc, x and y, or alternatively, its polar coordinates $\xi_0 = (x^2+y^2)^{1/2}$ and θ.

A plausible assumption is that the mass of the whole arriving jet m is sufficiently small, and the rate of propagation of the elastic waves along it is sufficiently large. Then, the whole jet can re-orient itself almost instantaneously to the direction of the applied force given by the angle $\theta = \alpha = \cos^{-1}[\mathrm{F}_x/(\mathrm{F}_x^2+\mathrm{F}_y^2)^{1/2}]$. In the plane $\theta = \alpha$ the jet configuration is given by the Euler–Bernoulli beam theory [26], with the jet assumed to be clamped at the tip and bent under the action of force $\mathbf{F}$ applied to its landing segment. Then, the jet configuration in space $x = X$, $y = Y$ and $z = Z$ is given by the following dimensionless expressions

$$\begin{aligned} &Z = H_1 - \frac{2^{1/2}}{(Qf)^{1/2}}\left[\sqrt{\cos\gamma_0} - \sqrt{\cos\gamma_0 - \cos\gamma}\right] \\ &\xi = \frac{1}{(2Qf)^{1/2}}\int_{\gamma}^{\pi/2}\frac{\cos\gamma}{\sqrt{\cos\gamma_0 - \cos\gamma}}\,\mathrm{d}\gamma \\ &X = \xi\cos\alpha, \quad Y = \xi\sin\alpha \end{aligned} \tag{5}$$

Here γ can be considered as a dummy variable, H_1 is the tip to collector distance rendered dimensionless by a, which is calculated as

$$H_1 = \left[\frac{2\cos\gamma_0}{fQ}\right]^{1/2} \tag{6}$$

and

$$f = (F_x^2 + F_y^2)^{1/2}, \quad Q = \frac{qea}{EI} \tag{7}$$

with E being an average Young's modulus of polymer solution in the jet, I being an average moment of inertia of the jet cross-section ($I = \pi b^4/4$, with b being an average cross-sectional radius in the jet), Q is the dimensionless parameter characterizing the ratio of the electrical and elastic forces involved.

The value of γ_0 in Eqs. (5) and (6) is determined by the following equation

$$\xi_0 = \frac{1}{(2Qf)^{1/2}} \int_{\gamma_0}^{\pi/2} \frac{\cos\gamma}{\sqrt{\cos\gamma_0 - \cos\gamma}} d\gamma \tag{8}$$

where ξ_0 is the current ξ coordinate of the landed jet segment on the disc rendered dimensionless by the disc radius a.

Its approximate solution with a sufficient accuracy is given by

$$\gamma_0 = \frac{\pi}{2} - \left[\frac{3}{4}\xi_0\sqrt{2Qf}\right]^{2/3} \tag{9}$$

The dimensional jet length L is calculated as

$$L = \frac{a}{(2Qf)^{1/2}} \int_{\gamma_0}^{\pi/2} \frac{d\gamma}{\sqrt{\cos\gamma_0 - \cos\gamma}} \tag{10}$$

Then, the jet mass $m = \rho\pi b^2 L$, with ρ being the polymer solution density.

5. Theoretical simulation results and discussion

The dimensionless parameter Q was taken as $Q = 1$. In the first case considered, the initial conditions for Eq. (4) were chosen as $t = 0$, $x = 0.3$, $y = 0.3$, $V_x = -0.5$, $V_y = 0.5$. The predicted overall jet configuration at different time moments is shown in Fig. 15a. In this case the jet length $L \approx a$ and $H_1 \approx 0.9$ (the corresponding dimensional value is $H \approx 0.9a$). The landing point of the jet moves over an almost circular path in the disc plane (Fig. 15b). The corresponding x and y coordinates are shown in Fig. 15c as functions of time. The corresponding period is approximately equal to 3.2. The latter means that the predicted dimensional frequency of such pendulum-like motion is equal to $\omega = (3.2)^{-1}[qe/(ma^2)]^{1/2}$. This value can be compared to the experimental data.

Another almost closed loop-like jet path over the disc is shown in Fig. 16. It corresponds to the following initial conditions: $t = 0$, $x = 0.3$, $y = 0.1$, $V_x = -0.5$, $V_y = 0.5$. Jet behavior corresponding to Figs. 15 and 16 could be characterized as a circular pendulum.

An interesting behavior corresponds to the initial conditions $t = 0$, $x = 0.9$, $y = 0.1$, $V_x = -0.5$, $V_y = 0.5$, which is depicted in Fig. 17. In this case, in distinction from the previous ones, the jet will produce a star-like deposit on the disc, which

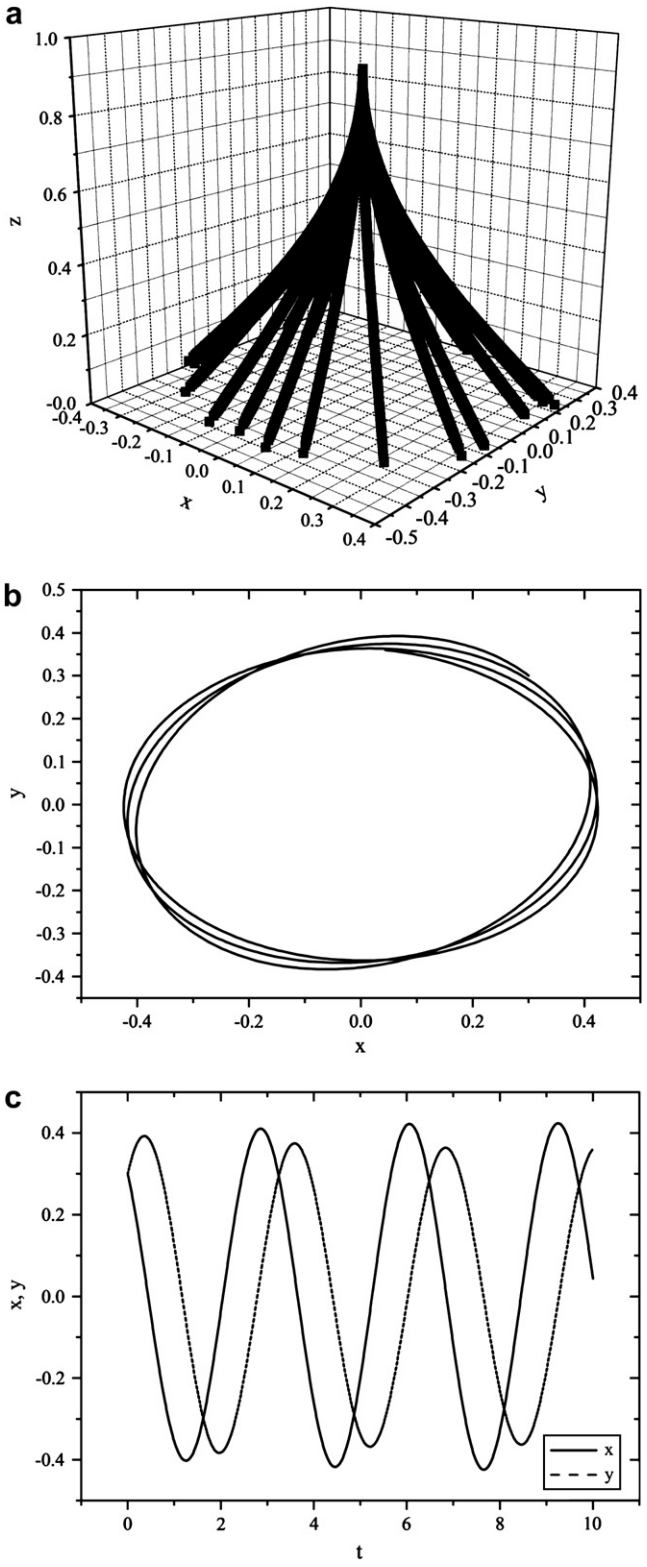

Fig. 15. Theoretically predicted pendulum-like motion of an electrified jet for the initial conditions $x = 0.3$, $y = 0.3$, $V_x = -0.5$, $V_y = 0.5$ at $t = 0$. (a) Three-dimensional configurations of the jet at several time moments (here and hereinafter the xyz coordinates are rendered dimensionless by a). This calculation ignores any Columbic interaction between the unrelaxed charge on the collector and the far away segments in Fig. 14. In fact, sometimes convex jet paths are observed. (b) The trajectory of the jet end on the horizontal motionless grounded electrode. (c) The horizontal coordinates of the jet end on the grounded electrode as functions of time; time is rendered dimensionless by T.

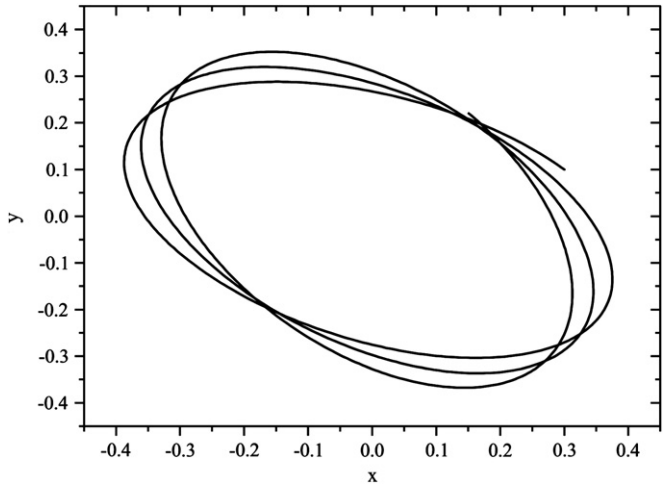

Fig. 16. Theoretically predicted pendulum-like motion of an electrified jet for the initial conditions $x = 0.3$, $y = 0.1$, $V_x = -0.5$, $V_y = 0.5$ at $t = 0$. The trajectory of the landing point of the jet on the horizontal motionless grounded electrode is shown.

is similar to the experimental observation in Fig. 3b in Ref. [27].

In the following, the theoretical predictions will be compared with the experimental data. In particular, the predicted and measured pendulum frequencies will be compared. According to Section 4, the dimensionless group Q (the ratio of the electrical to the elastic forces) determines the jet shape in the pendulum-like motion. For the value of $Q = 1$, we found $L \approx a$ and the dimensional $H \approx a$. For the estimates, it is reasonable to take $a \sim 1$ cm which agrees with the size of the grounded electrode in the experiments. Then, with $Q = 1$ the jet length L and the tip to collector distance H are both of the order of 1 cm. This is true for the jet image in Fig. 3. Therefore, the value of $Q = 1$ is reasonably accurate. Then, from Eq. (7) the product $qe = EI/a$. Taking as in Ref. [10] the elongational viscosity $\mu_{el} \sim 10^4$ g/(cm s), and the viscoelastic relaxation time $\Theta \sim 10^{-2}$ s, we can estimate the Young's modulus E as $E \sim \mu_{el}/\Theta \sim 10^6$ g/(cm s^2). Fig. 3 allows us to estimate the cross-sectional radius b of the jet as $b \sim 10^{-2}$ cm, and thus $I = \pi b^4/4 \sim 10^{-8}$ cm^4. With the values of the parameters listed, $qe = EI/a \sim 10^{-2}$ g cm^2/s^2. The total mass of the jet can be estimated as $m = \rho\pi b^2 L$, where ρ is the polymer density. Taking for the estimate $\rho \sim 1$ g/cm^3, and using the above-mentioned values of b and L, we find $m \sim 10^{-4}$ g. Then, the predicted frequency of the pendulum-like motion $\omega_{predicted} = (3.2)^{-1}[qe/(ma^2)]^{1/2} \approx 3$ Hz. This value is of the order of the lower bound of the experimental data for the measured frequency ω in Fig. 11.

According to the predictions in Fig. 15b, the dimensionless deposit radius in this case is $\xi_0 \approx 0.4$, which means that the predicted value of the deposit diameter $D = 2\xi_0 a \approx 1$ cm. This is of the order of the lower bound of the experimental data for D in Fig. 12.

It is of interest to estimate the values of q and e separately in addition to their product $qe \sim 10^{-2}$ g cm^2/s^2 estimated above. For an estimate of the electrical (convective) current I_{el} we take from Fig. 9 the value $I_{el} \sim 10$ μA $\sim 10^4$ g$^{1/2}$ cm$^{3/2}$/s^2. Let us assume that charge e corresponds to a jet section of the length $\ell \sim 10^{-1}$ cm above the grounded electrode, i.e. to the volume $\pi b^2 \ell \sim 10^{-5}$ cm^3 and denote the volumetric charge density in the jet as C, and the jet velocity as V. Then, $C = I_{el}(\ell/V)/[\pi b^2 \ell] = I_{el}/[\pi b^2 V]$. Therefore, $e = C\pi b^2 \ell = I_{el}\ell/V$. Let us take for the estimate $V = 10^3$ cm/s as in Fig. 13 and then, $e \sim 1$ g$^{1/2}$ cm$^{3/2}$/s. For comparison, the value of e in the computations of electrospinning used in Ref. [10] was $e = 8.48$ g$^{1/2}$ cm$^{3/2}$/s (the slightly higher value of e in Ref. [10] can be attributed to higher strengths of the electrical fields there). Then, $q \sim 10^{-2}/e \sim 10^{-2}$ g$^{1/2}$ cm$^{1/2}$/s. On the other hand, with no charge dissipation we would have $q_0 \sim e/(2\pi a) \sim 10^{-1}$ g$^{1/2}$ cm$^{1/2}$/s. Conduction of charge to the collector should be responsible for the reduction of q_0 to the level of q.

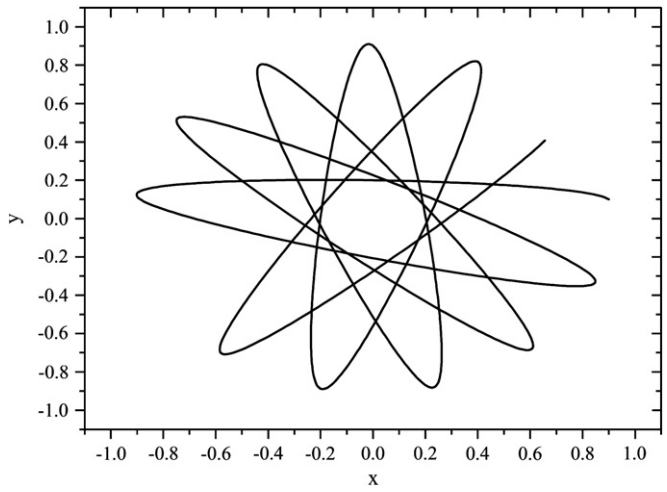

Fig. 17. Theoretically predicted pendulum-like motion of an electrified jet for the initial conditions $x = 0.9$, $y = 0.1$, $V_x = -0.5$, $V_y = 0.5$ at $t = 0$. The star-like trajectory of the jet end on the horizontal motionless grounded electrode is shown.

6. Conclusion

Pendulum-like rotation of short, almost straight, electrified jets was found experimentally. The characteristics of the rotation, in particular, the frequency of jet rotation about the vertical axis, were measured. The theoretical model proposed attributed the phenomenon of pendulum-like jet motion to the repulsive action between the charge on a landing segment of the jet and the electrical charges brought by the jet onto the grounded electrode but not immediately ''relaxed''. The comparison of the predicted and measured jet frequencies demonstrated a reasonable agreement.

Acknowledgement

We acknowledge financial support from the National Science Foundation, DMI-0403835-2 (NIRT), NSF subcontract 25-1110-0038-002 (Nebraska DMI-0600733), and a subcontract through Ohio State University, NSF EEC-0425626 (RF 60002999). The Coalescence Filtration Nanomaterials

Consortium of the University of Akron provided financial support and an industrial point of view. The authors thank Dr. Daniel Galehouse for the design and construction of a laser velocimeter, and Mr. Steven Roberts for technical support. DHR and TH thank Apogee Technology Inc. for financial support. ALY also acknowledges partial support of this work by the National Science Foundation under Grant NIRT CBET-0609062.

References

[1] Rayleigh Lord. The theory of sound. New York: Dover Publ.; 1945.
[2] Chandrasekhar S. Hydrodynamic and hydromagnetic stability. Oxford: Clarendon Press; 1961.
[3] Taylog GI. Proc R Soc London 1969;A313:453–75.
[4] Garmendia L. AIChE J 1977;23:935–8.
[5] Garmendia L, Smith IK. Can J Chem Eng 1975;53:606–10.
[6] Huebner AL, Chu HN. J Fluid Mech 1971;49:361–72.
[7] Tomita Y, Sudou K, Ishibashi Y. Bull JSME 1979;22:1390–8.
[8] Kirichenko VN, Petryanov-Sokolov IV, Suprun NN, Shutov AA. Sov Phys Dokl 1986;31:79–81.
[9] Spivak AF, Dzenis YA. Appl Phys Lett 1998;73:3067–9.
[10] Reneker DH, Yarin AL, Fong H, Koombhongse S. J Appl Phys 2000; 87:4531–47.
[11] Shin YM, Hohman MM, Brenner MP, Rutlege GC. Appl Phys Lett 2001; 78:1149–51.
[12] Feng JJ. Phys Fluids 2002;14:3912–26.
[13] Feng JJ. J Non-Newtonian Fluid Mech 2003;116:55–70.
[14] Caroll CP, Joo YK. Phys Fluids 2006;18:053102.
[15] Yarin AL, Koombhongse S, Reneker DH. J Appl Phys 2001;89:3018–26.
[16] Hohman MM, Shin M, Rutledge G, Brenner MP. Phys Fluids 2001; 13:2221–36.
[17] Frenot A, Chronakis IS. Curr Opin Colloid Interface Sci 2003;8:64–75.
[18] Huang ZM, Zhang YZ, Kotaki M, Ramakrishna S. Compos Sci Technol 2003;63:2223–53.
[19] Dzenis Y. Science 2004;304:1917–9.
[20] Ramakrishna S, Fujihara K, Teo WE, Lim TC, Ma Z. An introduction to electrospinning of nanofibers. Singapore: World Scientific; 2005.
[21] Reneker DH, Yarin AL, Zussman E, Xu H. Adv Appl Mech 2007;41:43–195.
[22] Saville DA. Phys Fluids 1971;14:1095–9.
[23] Yarin AL, Kataphinan W, Reneker DH. J Appl Phys 2005;98:064501.
[24] Han T, Reneker DH, Yarin AL. Polymer 2007;48:6064–76.
[25] Abramowitz M, Stegun IA. Handbook of mathematical functions. New York: Dover Publ.; 1972.
[26] Landau LD, Lifshits EM. Theory of elasticity. New York: Pergamon Press; 1975.
[27] Sun D, Chang C, Li S, Lin L. Nano Lett 2006;6:839–42.